

# Cascaded and Separate Channel Estimation based on CNN for RIS-MIMO Systems

## Wala'a Hussein

Department of Computer and Communication Systems Engineering, Faculty of Engineering, Universiti Putra Malaysia, Malaysia | Department of Chemical Engineering and Petroleum Refining, Basrah University for Oil and Gas, Iraq | Department of Computer Technology Engineering, Faculty of Engineering, Iraq University College, Iraq  
walaahussein613@gmail.com (corresponding author)

## Nor K. Noordin

Department of Computer and Communication Systems Engineering, Faculty of Engineering, Universiti Putra Malaysia, Malaysia | Wireless and Photonics Networks Research Center of Excellence (WiPNET), Faculty of Engineering, Universiti Putra Malaysia, Malaysia  
nknordin@upm.edu.my (corresponding author)

## Kamil Audah

Department of Computer and Communication Systems Engineering, Faculty of Engineering, Universiti Putra Malaysia, Malaysia | Department of Electronics Technologies, Southern Technical University, Iraq  
thegenusnabster@gmail.com

## Mod Fadlee B. A. Rasid

Department of Computer and Communication Systems Engineering, Faculty of Engineering, Universiti Putra Malaysia, Malaysia | Wireless and Photonics Networks Research Center of Excellence (WiPNET), Faculty of Engineering, Universiti Putra Malaysia, Malaysia  
fadlee@upm.edu.my

## Alyani Binti Ismail

Department of Computer and Communication Systems Engineering, Faculty of Engineering, Universiti Putra Malaysia, Malaysia | Wireless and Photonics Networks Research Center of Excellence (WiPNET), Faculty of Engineering, Universiti Putra Malaysia, Malaysia  
alyani@upm.edu.my

## Aymen Flah

MEU Research Unit, Middle East University, Jordan | Applied Science Research Center, Applied Science Private University, Jordan  
flahaymening@yahoo.fr

Received: 15 April 2024 | Revised: 25 April 2024 | Accepted: 27 April 2024

Licensed under a CC-BY 4.0 license | Copyright (c) by the authors | DOI: <https://doi.org/10.48084/etasr.7499>

## ABSTRACT

With the dramatic increase in mobile users and wireless devices accessing the network, the performance of 5G wireless communication systems is severely challenged. Reconfigurable Intelligent Surface (RIS) has received much attention as one of the promising technologies for 6G due to its ease of deployment, low power consumption, and low price. This study aims to improve accuracy, reliability, and the capacity to estimate channel characteristics between transmitter and receiver. However, this is practically challenging for the following reasons. Due to the lack of active components for baseband signal processing, low-cost passive RIS elements can only reflect incident signals but without the capability to transmit/receive pilot signals for channel estimation as active transceivers in conventional wireless communication systems. This

study presents different channel estimation methods for RIS-MIMO systems that use deep learning techniques.

**Keywords-channel estimation; deep learning; RIS-MIMO; beamforming; phase shift**

## I. INTRODUCTION

Reconfigurable Intelligent Surfaces (RIS) have attracted a lot of attention [1]. RIS technology is used in many sectors, including secure communications, UAVs, and energy efficiency [2-5]. The source node (BS) is equipped with  $N$  antennas, joint phase shift optimization at the RIS element, and beamforming optimization at the same time. This optimization process relies on acquiring channel state information for all connections. Separate channels are utilized for BS  $\rightarrow$  RIS and RIS  $\rightarrow$  UE links, while cascaded channels are employed for end-to-end BS  $\rightarrow$  RIS  $\rightarrow$  UE links. Estimating individual BS  $\rightarrow$  RIS and RIS  $\rightarrow$  UE channels poses a challenge. However, it is feasible to estimate these channels with some degree of ambiguity [7]. In [8], the tensor model technique was employed to estimate separate channels within the MIMO RIS network. In [9], an iterative approach was followed to compute these individual channels. On the contrary, estimating the cascaded BS  $\rightarrow$  RIS  $\rightarrow$  UE channels is comparatively more straightforward.

In [10, 11], cascaded channel estimation was proposed for various scenarios, including the Single-Input Single-Output (SISO) scenario (a single antenna employed on both the transmitter and receiver sides), double RISs, and Multiple-Input Single-Output (MISO) RIS-assisted network. Additionally, in [12], cascaded channel estimation was achieved in the MIMO-OFDM situation applying deep learning algorithms. The estimation of the cascaded channels often leads to problems. Analyzing the total channel capacity in cascade scenarios becomes intricate, especially when dealing with multiple antennas at both the transmitter and the receiver. However, the estimation of separate channels presents unique difficulties. On the other hand, more well-established technologies include integrated phase shift and beamforming techniques. This study suggests combining cascaded and separate channel approaches with phase shift and beamforming. Previous studies [8, 9] have shown that it is possible to optimize beamforming and phase corrections simultaneously for RIS-assisted MIMO networks utilizing individual channel estimates. In [13], the optimization of phase adjustment in cascaded channels was addressed when beamforming was not necessary on the transmitter side of the SISO-RIS system. In [14], further research on RIS-MIMO beamforming was carried out deploying the cascaded channel and iterative beamforming/phase correction execution.

Beamforming and phase shifts in MIMO-RIS networks must be fine-tuned using iterative optimization techniques. Because of concerns about convergence, this further increases the demand for online computations and makes implementation more complicated. Maintenance of constant amplitude gains across different phase shifts simplifies the optimization procedure. Optimization becomes more complicated when this requirement is not met [15, 16].

Emerging developments in the field of machine learning provide appealing substitutes for the RIS phase transition [17]. This study presents a new deep-learning architecture employing two interconnected neural networks. Each network is specifically trained to address the distinct channel characteristics encountered in two scenarios. Compared to traditional reinforcement learning approaches, the proposed double neural network exhibits exceptional performance, even in scenarios with a large number of RIS components. A 5G link level-based RIS-MIMO MATLAB 2023a simulator was utilized to model the time-frequency response of the channel as a 2D picture and Anaconda Spyder for training on the dataset.

## II. SYSTEM AND CHANNEL MODELS

Figure 1 depicts the passive/hybrid RIS architecture in conjunction with MIMO communication systems based on a limited number of RF chains.

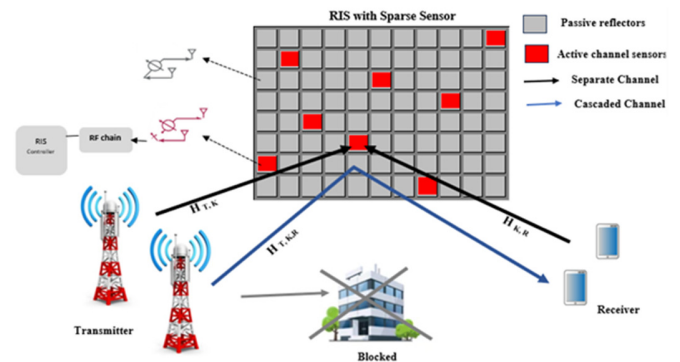


Fig. 1. The proposed RIS design uses a surface-distributed array of  $K$  active/passive channel sensors. These sensors operate in two modes: (i) a channel sensing mode connected to the baseband for channel estimation and (ii) a reflection mode applying phase shifts to incident signals. The remaining RIS elements are passive reflectors without baseband connections.

In scenarios where direct communication between the source (BS) and the destination (UE) nodes is impeded by severe obstruction or is blocked, the channel efficiency from the  $n^{\text{th}}$  antenna at the BS to the  $k^{\text{th}}$  element of the RIS experiences Rician fading, as outlined below:

$$H_{T,K} = \sqrt{\frac{k_{k,n}}{k_{k,n}+1}} h_{k,n}^{(LOS)} + \sqrt{\frac{k_{k,n}}{k_{k,n}+1}} h_{k,n}^{(NLOS)} \quad (1)$$

where  $k_{k,n}$  represents the Rician factor respective link, and  $h_{k,n}^{(LOS)}$  and  $h_{k,n}^{(NLOS)}$  are the components of the Rician fading channel for Line Of Sight (LOS) and Non Line Of Sight (NLOS). The expression for the LOS component is as follows:

$$h_{k,n}^{(LOS)} = \sqrt{\beta_0} e^{-j(k-1)\pi \sin\theta} d_{k,n}^{\frac{-\alpha}{2}} \quad (2)$$

In this equation,  $\theta$  denotes the angle of arrival at the RIS, and  $\beta_0$  represents the path loss at the reference distance of 1 m. In the NLOS scenario:

$$h_{k,n}^{(NLOS)} = \tilde{h}_{k,n} d_{k,n}^{-\frac{\alpha}{2}}$$

where  $\tilde{h}_{k,n}$  is the complex Gaussian small-scale fading with a unit variance, and zero mean is denoted by  $H_{K,R}$ . Similarly, the channel connecting the  $k^{\text{th}}$  RIS elements and the  $m^{\text{th}}$  antenna at the UE is denoted as  $H_{K,R}$ . The signal received at the destination is expressed as:

$$Y = H_{T,K} \Theta H_{K,R} x + n \quad (3)$$

In this context,  $Y$  belongs to the  $C^{M \times 1}$ ,  $H_{T,K} \in C^{N \times K}$  is the channel matrix between UE and RIS, and  $H_{K,R} \in C^{M \times K}$ , is the channel matrix representing the communication link between the RIS and UE. Additionally,  $n$  belongs to the  $C^{M \times 1}$  space and signifies the additive noise between the BS and RIS, and the phase shift matrix at the RIS is represented as  $\Theta$ , which is given by:

$$\Theta = \text{diag}(a_1 e^{j\theta_1} \dots \dots, a_k e^{j\theta_k}) \quad (4)$$

In this context,  $a_k$  signifies the amplitude, and  $\theta_k$  represents the phase shift at the  $k^{\text{th}}$  elements. Although  $\theta_k$  is typically presumed to remain constant in numerous existing methodologies, it is also acknowledged that it can be subject to variation.

#### A. Cascaded Channel Estimation Scenario

Cascaded channel estimation aims to capture the combined influence of the BS-RIS and RIS-UE channels in a single step. When employing fully passive RIS without sensing devices, it becomes impractical to estimate the BS-RIS and RIS-UE channels separately. Instead, only the combined BS-RIS-UE channel can be estimated, typically at one endpoint, such as the UE, in the downlink communication system. For passive RIS, direct estimation is limited to the overall BS-RIS-UE channel. Separate channel estimates require additional capabilities at the RIS, typically at the UE, in the downlink communication system. During time slot  $t$ , the BS transmits pilot signals, and the properties of the signal received by the UE can be described by:

$$y_{UE}^{(t)} = \sum_{k=1}^K \sqrt{P_{BS}} H_{T,K} \theta^{(t)} H_{K,R} x_k^{(t)} + \eta_{UE}^{(t)} \quad (5)$$

where  $x_k^{(t)} \in C^{M_U \times 1}$  represents the transmitted signal of the pilot by the BS,  $\theta^{(t)} = \text{diag}(\theta^{(t)})$  is represented as a diagonal reflection matrix during time slot  $t$  at RIS, and the AWGN at the user can be represented as  $\eta_u^{(t)} \in C^{M_u \times 1}$ . Using the product properties of Khatri-Rao the following equation can be derived:

$$\text{vec}(H_{T,K} \theta^{(t)} H_{K,R}) = \underbrace{H_{K,R}^T}_{\bar{H}_k} \odot H_{T,K} \theta^{(t)}, \quad k = 1..K \quad (6)$$

In this expression,  $\bar{H}_k \in C^{M_B M_u \times N}$  signifies the cascaded channel of user  $k$ ,  $\text{vec}(\cdot)$  denotes vectorization, and  $\odot$  denotes the Khatri-Rao product.

#### B. Separate Channel Estimation Scenario

Unlike the combined channel estimation approach, the separate channel estimation approach treats the transmitter-to-RIS (BS-RIS) and RIS-to-receiver (RIS-UE) channels as independent and estimates them individually. This method is particularly applicable in scenarios with semi-passive or hybrid RIS equipped with dedicated sensing devices (Ns). When such sensing devices are available, they can be used to estimate the individual channels between the BS or UE and the RIS using dedicated pilot signals sent by either the BS or UE. Channel estimation is conducted at the RIS. TDD systems can effectively leverage channel reciprocity to obtain the Channel State Information (CSI) from the RIS to the BS or UE. This is because the same channel is deployed for transmission in both directions. Applying this method in Frequency-Division Duplexing (FDD) systems is complex. FDD engages separate frequencies for transmission and reception, eliminating channel reciprocity. To reduce hardware costs in semi-passive RIS, a limited number of low-resolution Analog-to-Digital Converters (ADCs) might be employed. However, this necessitates active sensors on the RIS, capable of transmitting and receiving pilots for channel estimation in FDD systems, leading to increased power consumption. Specifically, the channels from the BS and UE to the Ns sensing devices are represented as follows:  $\check{G}(H_{T,K}) \in C^{N_s \times M_B}$  and  $\check{H}(H_{K,R}) \in C^{N_s \times N_U}$ , respectively. Additionally,  $X_B \in C^{M_B \times T}$  and  $X_U \in C^{N_U \times T}$  represent the pilot sequences transmitted by the BS and UE, in which the channel sensing period is represented by  $T$  pilot symbols. Hence, the following is a possible expression for the signal received at the Ns sensing devices:

$$Y_S = \mathbb{Q}(\sqrt{P_B} \check{G} X_B + \sum_{k=1}^K \sqrt{P_U} \check{H}_k X_U + \eta_S) \quad (7)$$

where  $\mathbb{Q}(\cdot)$  is the quantization function that depends on the precision of the ADCs. The transmit power at the BS and the UE can be represented as  $P_B$  and  $P_u$ , respectively. The AWGN at the sensing devices is represented as  $\eta_S \in C^{N_s \times T}$ . This is particularly advantageous in millimeter-wave [18] or THz [19] frequency bands.

### III. JOINT PHASE SHIFT AND BEAMFORMING

#### A. Cascaded Channel

In a fully passive RIS scenario, estimating the combined effect of the BS and the RIS on the signal requires considering both the beamforming applied at the BS and the phase shifts introduced by the RIS elements. This combined influence is reflected in the received signal at the UE, which can be expressed mathematically as:

$$Y_{UE} = F \phi \mathbf{1}_F x + \eta \quad (8)$$

where  $\phi = \text{diag}(\phi_v, \dots, \phi_v) \in C^{NK \times NK}$ , and  $\mathbf{1}_F = [1_1^T, \dots, 1_1^T]$ . The matrix  $\mathbf{1}_n$  is a  $K \times N$  matrix where in the  $n^{\text{th}}$  column, all elements are set to one and all other elements are set to zero. The beamforming at the BS can be derived as:

$$x = Ws \quad (9)$$

where  $W = [w_1, \dots, w_Q]$ , where,  $w_q$  represents the  $q^{\text{th}}$  beamforming vector, and  $s = [s_1, \dots, s_Q]^T$ , where  $s_q$  signifies

the  $q^{\text{th}}$  transmit data, with the assumption that  $E[s_q^2] = 1$  for all  $q$ . Upon substituting (8) into (9), we obtain:

$$Y_{UE} = F\phi 1_F Ws + \eta \quad (10)$$

The joint optimization of beamforming and phase shifting aims to maximize the capacity of the channel between the source (S) and destination (D), as:

$$\max_{W, \phi_v} C = \log \det \left| I + \frac{AWW^H A^H}{\sigma^2} \right| \quad (11)$$

where  $A = F\phi 1_F \in \mathbb{C}^{M \times N}$ . The Singular Value Decomposition (SVD) of matrix  $A$  can be represented as  $A = U\tilde{V}^H$ , where  $U$  is a matrix in  $\mathbb{C}^{M \times M}$  representing the left singular vectors,  $\tilde{V}$  is a matrix in  $\mathbb{C}^{N \times N}$  representing the right singular vectors, and  $\tilde{\sim}$  is a matrix in  $\mathbb{C}^{M \times N}$  representing the singular values. When  $\phi_v$  is fixed, the optimal beamforming vectors are:

$$w_q = \sqrt{P_q} v_q, \quad q = 1, 2, \dots, Q \quad (12)$$

Consider  $v_q$  as the right singular vector of  $q^{\text{th}}$  in  $\tilde{V}$ , and  $P_q$  denoting the power allocated for the transmit data of  $q^{\text{th}}$  to ensure the satisfaction of the transmit power constraint  $\sum_{q=1}^Q P_q \leq P_s$  obtained through water-filling. Substituting (12) can give:

$$\max_{p_{hi}} C = \log \det \left| I + \frac{P \tilde{\sim} \tilde{\sim}^H}{\sigma^2} \right| \quad (13)$$

where  $P = \text{diag}[P_1, \dots, P_Q, \underbrace{0, \dots, 0}_{M-Q}]$ .

To achieve the highest possible system capacity, the cascaded network undergoes training. This is achieved through the minimization of the negative values of the network's outputs, essentially aiming for the most positive values:

$$\min \{ \sum_{l=1}^L (C^{(l)} - C_{F(l), \phi(l)})^2 \} \quad (14)$$

### B. Separate Channel

This section focuses on designing the phase control matrix at the RIS and the beamforming vectors for both the BS and UE when separate estimation of the BS to RIS (BS-RIS) and RIS to UE (RIS-UE) channels, denoted by  $H_{T,K}$  and  $H_{K,R}$  respectively, is performed using a semi-passive RIS. The equation representing the signal received at the RIS's sensing devices ( $N_s$ ) is given by:

$$Y_{N_s} = y_{BS} + y_{UE} \quad (15)$$

$$y_{RIS}^{(t)} = \sum_{k=1}^K \sqrt{P_{BS}} H_{T,K} \theta^{(t)} x_k^{(t)} + \eta_s^{(t)} \quad (16)$$

$$y_{RIS}^{(t)} = \sum_{k=1}^K \sqrt{P_{UE}} H_{K,R} \theta^{(t)} x_k^{(t)} + \eta_s^{(t)} \quad (17)$$

Assume a diagonal matrix  $\phi$  of size  $MKN \times MKN$  with all diagonal elements equal to  $\phi_v$ , represented as:

$$\phi = \text{diag}(\phi_v, \dots, \phi_v) \in \mathbb{C}^{MKN \times MKN}$$

Let  $x_{BS}$  and  $x_{UE}$  denote the pilot sequences transmitted by the BS and UE, respectively.  $T$  represents the number of pilot symbols transmitted during the channel sensing period. The beamforming matrix at the sensing device, denoted by  $N_s$  can be obtained as:

$$x_{N_s} = x_{BS} + x_{UE} \quad (18)$$

$$x = Ws \quad (19)$$

The objective of jointly optimizing beamforming and phase shifting is to maximize the capacity of the channel between the S and D, where  $W$  represents the  $q^{\text{th}}$  beamforming vector and  $s$  denotes the  $q^{\text{th}}$  transmit data from both S and D.

$$\max_{W, \phi_v} C = \frac{1}{K} \sum_{k=1}^K \log_2 (1 + \text{SNR} | (h_{T,K} \odot h_{K,R})^T \phi |^2) \quad (20)$$

The uplink channels from the transmitter and receiver to the RIS at the  $k^{\text{th}}$  subcarrier are denoted as  $H_{T,K}$  and  $H_{K,R}$ , respectively. Leveraging reciprocity, the downlink channels from the RIS to the transmitter and receiver are given by the transposes  $H_{T,K}^T, H_{K,R}^T$ . With this notation, the received signal at the receiver can be expressed as:

$$y_{UE} = H_{K,R}^T \odot H_{T,K} x_k + \eta_k \quad (21)$$

## IV. DEEP LEARNING MODEL DESIGN FOR OPTIMAL PHASE SHIFT AND HIGH-CAPACITY DATA RATE

### A. Deep Learning Structure

The updated deep learning model employs two distinct neural networks, Net1 and Net2, as observed in Figure 2. Net1 is the main operating network. The system's inputs, which are  $N \times M \times K$ , stand for each item in a collection of  $2^R$  dimensional category vectors that are cascaded  $K$  times. There is one RIS element for every set of  $R$  bits, and each set indicates a different phase shift.

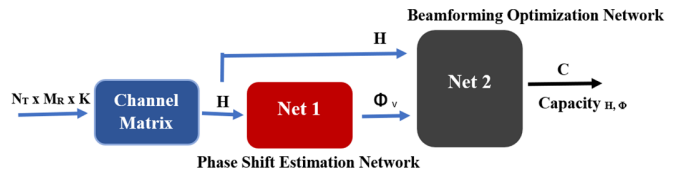


Fig. 2. The deep learning network structure.

The primary network Net1 is trained indirectly by combining Net1 and Net2 to create a powerful learning pipeline of cascaded networks. This pipeline trains without the need for labeled data by minimizing the negative of its final output. After the training phase, Net1 generates phase shifts to maximize the network capacity for a given channel (represented as  $F$ ). With these optimal phase shifts, the ideal beamforming configuration at the source is determined by (12). Net2 efficiently processes the channel information ( $F$ ) and the precoding matrix  $\phi_v$  to directly estimate the resulting channel capacity  $C_F, \phi$ .

### B. The Training Phase of Deep Neural Networks

Algorithm 1 describes the training phase of Net1 and Net2 for cascaded and separate channel estimation.

ALGORITHM 1: TRAIN NET1 AND NET2 FOR CASCADED AND SEPARATE CHANNEL ESTIMATION

Procedure:

1. Generate the dataset by scenario 1, from  $N \times K \times M$ , then obtain the least square channel matrix  $H_{T,K,R}$  (BS-RIS-UE),  $H_{T,K}$ , and  $H_{K,R}$  (BS-RIS, RIS-UE), and the random phase shift control matrix  $\Phi_v$ .

2. Train Network 1

Input: 40,000 frames channel matrix  $H_{LS(T,K,R)}$ , true phase shift  $\Phi_{True}$ , and random phase shift  $\Phi_v$ .

$i = 0$  (initial epoch)

Initialize optimizer = Adam

While  $i < 600$  (max epochs)

Obtain the equivalent channel matrix from F and  $\Phi$

$$A = F \text{diag}(\phi_1, \dots, \phi_v) 1_F$$

Obtain optimal phase control matrix  $\Phi_v$

$i = i + 1$

End While

Return  $\Phi$

Output:  $\Phi_v$  (estimated optimal phase shifts)

3.Cascade Net1 with Net2 after training Net1

4. Train Network 2

Input: 40,000 frames channel matrix  $H_{LS(T,K,R)}$  optimal phase shift matrix  $\Phi_v$

$i = 0$  (initial epoch)

Initialize optimizer = Adam

Initialize loss function = MSE

While  $i < 600$  (max epochs)

Obtain the equivalent channel matrix from F and  $\Phi$

$$A = F \text{diag}(\phi_1, \dots, \phi_v) 1_F$$

Utilize the water-filling algorithm to determine the transmit power  $P$

Obtain the capacity as

$$\max_{W, \Phi_v} C = \log \det \left[ I + \frac{AWW^H A^H}{\sigma^2} \right] \quad (11)$$

where  $A = F \Phi 1_F \in \mathbb{C}^{M \times N}$

Calculate the loss function as

$$\min \left\{ \sum_{l=1}^L (C^{(l)} - C_{F(l), \Phi(l)})^2 \right\} \quad (14)$$

$i = i + 1$

End While

Return  $C$

Output:  $C_{F, \Phi}$  (corresponding capacity)

End Procedure

V. SIMULATION RESULTS

An RIS-supported network was tested, in which  $M = 2$ , two-antenna users were linked to two BSs equipped with  $N = 2$  antennas via a RIS with  $K_{active} = 8$  and  $K_{passive} = 80$  components. All simulations presented below assume that the channels undergo Rician fading with a Rician factor  $K_{k,n}$  of 10 dB. Additionally, the phase shifts at each RIS element are quantized using three bits. Figure 3 demonstrates the capacities of the RIS-MIMO network, where both the source and destination are equipped with multiple antennas. The results portrayed are for RIS configurations with varying numbers of elements, specifically 8, 32, and 64. Figure 3 indicates that the data rates achieved by both the cascade and separate channels are high, which is an amazing performance considering the signal-to-noise ratio.

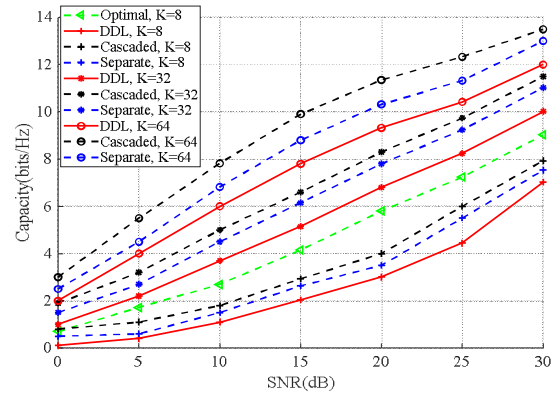


Fig. 3. Contrasts the RIS-MIMO network's capabilities for ideal channels with varying amounts of  $K$  elements, cascaded, separable, and double deep learning.

Figures 4 and 5 illustrate the normalized path loss performance across various observation angle values with  $K=8$ , exhibiting a similar trend. The simulation parameters are consistent with Figure 3. The spatial correlation in  $H$  is greater at  $a = \lambda/2$  compared to when  $a = \lambda/5$  gives better performance. However, when the distance  $a$  is equal to the wavelength  $\lambda$ , the path loss is notably high, albeit less than in the case of  $a = \lambda/2$  wavelength, and it represents the worst performance compared to a wavelength of  $4\lambda$ . The proposed technique is advantageous in both cases, leading to higher-quality estimated channels. However, the route loss is quite large when the distance  $a$  is equal to the wavelength  $\lambda$ , but it is lower than when  $a = \lambda/2$ , and it is the worst performance when compared to a wavelength of  $4\lambda$ . Positioning the reconfigurable intelligent surfaces either near the source or far from the destination results in a very high level of overall channel gain. The channel gain is maximum when the reflecting surface is close to the source or target, or when the distance between the RIS source and the RIS destination is zero. Figure 7 manifests the difference between LOS and NLOS. The data rate was also calculated. For the first scenario, the data rate is extremely high when employing LOS, presuming there is no obstruction between the sender and the receiver.

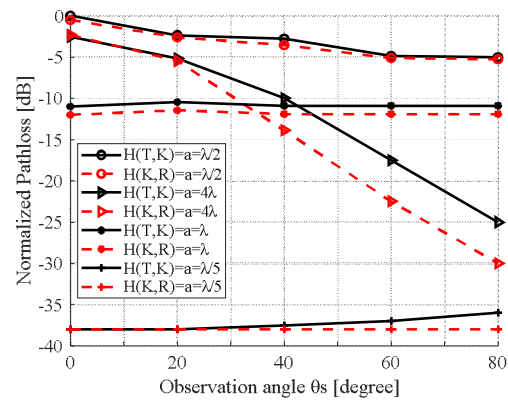


Fig. 4. The normalized path loss for two separate channels when the area between the node and another node (meta-atom  $a$ ) is equal to  $4\lambda$ ,  $\lambda$ ,  $\lambda/2$ , and  $\lambda/5$  incoming wavelength with different degrees of angle  $\theta_s$ .

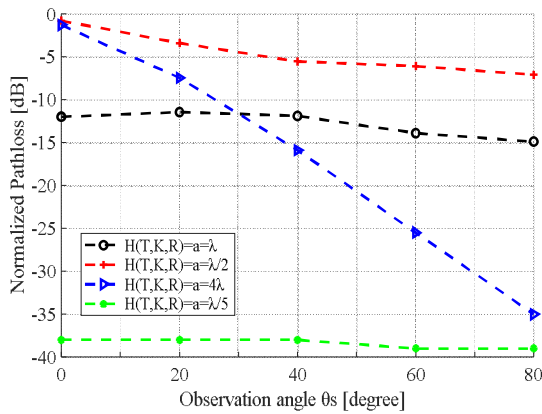


Fig. 5. Normalized path loss for cascaded channels when the area between the node and another node (meta-atom  $a$ ) is equal to  $4\lambda$ ,  $\lambda$ ,  $\lambda/2$ , and  $\lambda/5$  incoming wavelengths with different degrees of angle  $\theta_s$ .

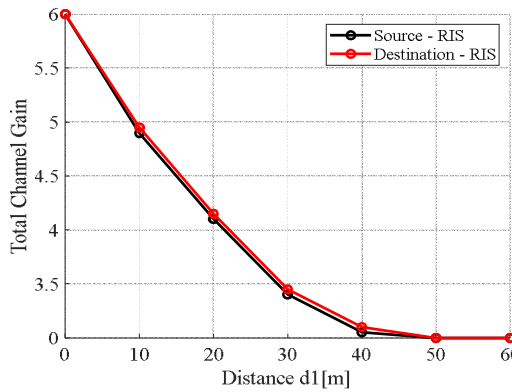


Fig. 6. The total channel gain depends on the distance of the source and destination from the RIS.

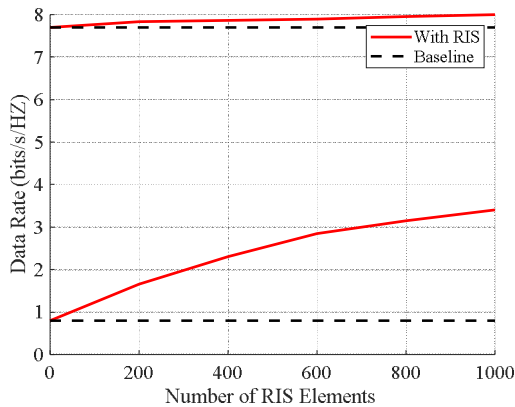


Fig. 7. Path LOS and NLOS with RIS and direct path.

The second scenario employs the reflecting surface method while utilizing NLOS technology, assuming that there is an obstruction preventing a direct path between the transmitter and the receiver. In this case, the use of reflecting surfaces has a noticeable impact. The results disclose that the proposed reflected surfaces yield a higher data rate than the standard surface. Figure 8 compares the performance of various PSBA-based separate channel estimator architectures, such as CBDNet [20], GAN-CBDN [21], CV-DnCNN [22], and

MDRN [21], against conventional channel estimating methods, including ADMM [23] and PARAFAC [24]. The results of the simulations were averaged over 400 iterations for the proposed method. Notably, both PSBA- $H_{K,R}$  and PSBA- $H_{T,K}$  exhibit superior NMSE performance compared to GAN-CBD and CBDNet by 5.63 and 4.51 dB, respectively. Additionally, when compared to CV-DnCNN, which also employs CNN, along with traditional ADMM and PARAFAC methods, PSBA demonstrates lower complexity while achieving comparable NMSE performance.

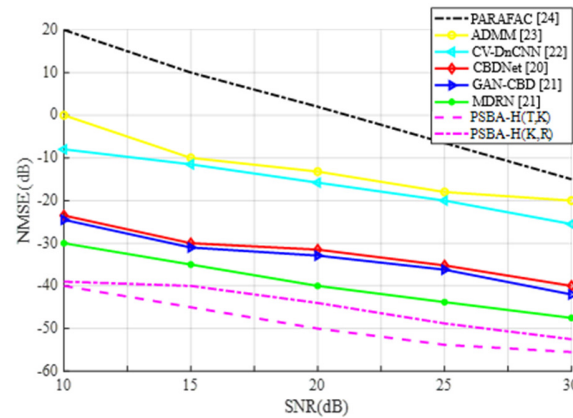


Fig. 8. Comparison of NMSE performance among ADMM, CV-DnCNN, CBDNet, GAN-CBD, and MRDN using separate CS methods.

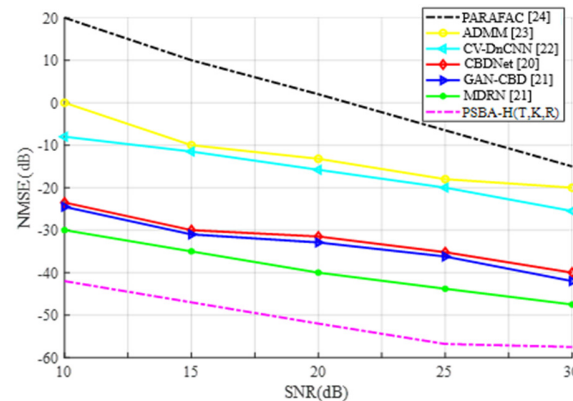


Fig. 9. Comparison of NMSE performance among ADMM, CV-DnCNN, CBDNet, GAN-CBD, and MRDN using cascaded CS methods.

Figure 9 compares various models, namely MRDN, CBDNet, and GAN-CBD. It can be observed that PSBA- $H_{T,K,R}$  shows superior NMSE performance and faster convergence compared to other models. This advantage stems from its network judgment capability, which outperforms PSBA- $H_{T,K}$  and PSBA- $H_{K,R}$ . Additionally, PSBA- $H_{T,K,R}$  offers reduced computational complexity in training and offline operation, leading to enhanced robustness of the channel estimator across different scenarios. The average running time of PSBA- $H_{T,K,R}$  is 0.0073 s, while PSBA- $H_{T,K}$  and PSBA- $H_{K,R}$  exhibit running times of 0.0096 and 0.0092 s, respectively. Furthermore, the computational complexity in both training and offline operations for PSBA- $H_{T,K,R}$  is lower than that of PSBA- $H_{T,K}$  and PSBA- $H_{K,R}$ .

## VI. CONCLUSION AND FUTURE WORK

This study presented a DL network that simultaneously optimizes phase shifts and beamforming in the RIS-MIMO system, taking into account cascaded and separate channels. A two-stage channel estimate approach was proposed for the RIS-MIMO communication system, with the first stage estimating the cascaded channel between the BS-RIS-UE and the second stage estimating the separate channels between the BS-RIS and the RIS-UE. Then, to make the most of the user's channel gain, a phase shift design and a beamforming approach were demonstrated for the RIS. The incorporation of RIS into bands with higher frequencies, such as the THz band, also poses a formidable obstacle. More accurate channel estimate algorithms are needed to guarantee dependable communication while deploying RIS in complex and dynamic contexts, such as cities with many buildings, moving cars, or satellite communications [25].

## REFERENCES

- [1] M. Jian *et al.*, "Reconfigurable intelligent surfaces for wireless communications: Overview of hardware designs, channel models, and estimation techniques," *Intelligent and Converged Networks*, vol. 3, no. 1, pp. 1–32, Mar. 2022, <https://doi.org/10.23919/ICN.2022.0005>.
- [2] S. Fang, G. Chen, and Y. Li, "Joint Optimization for Secure Intelligent Reflecting Surface Assisted UAV Networks," *IEEE Wireless Communications Letters*, vol. 10, no. 2, pp. 276–280, Oct. 2021, <https://doi.org/10.1109/LWC.2020.3027969>.
- [3] C. Cao, Z. Lian, Y. Wang, Y. Su, and B. Jin, "A Non-Stationary Geometry-Based Channel Model for IRS-Assisted UAV-MIMO Channels," *IEEE Communications Letters*, vol. 25, no. 12, pp. 3760–3764, Sep. 2021, <https://doi.org/10.1109/LCOMM.2021.3116192>.
- [4] C. Huang, G. C. Alexandropoulos, A. Zappone, M. Debbah, and C. Yuen, "Energy Efficient Multi-User MISO Communication Using Low Resolution Large Intelligent Surfaces," in *2018 IEEE Globecom Workshops (GC Wkshps)*, Abu Dhabi, United Arab Emirates, Dec. 2018, pp. 1–6, <https://doi.org/10.1109/GLOCOMW.2018.8644519>.
- [5] S. Fang, G. Chen, Z. Abdullah, and Y. Li, "Intelligent Omni Surface-Assisted Secure MIMO Communication Networks With Artificial Noise," *IEEE Communications Letters*, vol. 26, no. 6, pp. 1231–1235, Jun. 2022, <https://doi.org/10.1109/LCOMM.2022.3159575>.
- [6] H. Zhang *et al.*, "Channel Estimation With Hybrid Reconfigurable Intelligent Metasurfaces," *IEEE Transactions on Communications*, vol. 71, no. 4, pp. 2441–2456, Apr. 2023, <https://doi.org/10.1109/TCOMM.2023.3244213>.
- [7] Z. Q. He and X. Yuan, "Cascaded Channel Estimation for Large Intelligent Metasurface Assisted Massive MIMO," *IEEE Wireless Communications Letters*, vol. 9, no. 2, pp. 210–214, Feb. 2020, <https://doi.org/10.1109/LWC.2019.2948632>.
- [8] G. T. de Araújo, A. L. F. de Almeida, and R. Boyer, "Channel Estimation for Intelligent Reflecting Surface Assisted MIMO Systems: A Tensor Modeling Approach," *IEEE Journal of Selected Topics in Signal Processing*, vol. 15, no. 3, pp. 789–802, Apr. 2021, <https://doi.org/10.1109/JSTSP.2021.3061274>.
- [9] J. Mirza and B. Ali, "Channel Estimation Method and Phase Shift Design for Reconfigurable Intelligent Surface Assisted MIMO Networks," *IEEE Transactions on Cognitive Communications and Networking*, vol. 7, no. 2, pp. 441–451, Jun. 2021, <https://doi.org/10.1109/TCCN.2021.3072895>.
- [10] C. You, B. Zheng, and R. Zhang, "Wireless Communication via Double IRS: Channel Estimation and Passive Beamforming Designs," *IEEE Wireless Communications Letters*, vol. 10, no. 2, pp. 431–435, Oct. 2021, <https://doi.org/10.1109/LWC.2020.3034388>.
- [11] G. Zhou, C. Pan, H. Ren, K. Wang, and A. Nallanathan, "A Framework of Robust Transmission Design for IRS-Aided MISO Communications With Imperfect Cascaded Channels," *IEEE Transactions on Signal Processing*, vol. 68, pp. 5092–5106, 2020, <https://doi.org/10.1109/TSP.2020.3019666>.
- [12] S. Liu, M. Lei, and M. J. Zhao, "Deep Learning Based Channel Estimation for Intelligent Reflecting Surface Aided MISO-OFDM Systems," in *2020 IEEE 92nd Vehicular Technology Conference (VTC2020-Fall)*, Victoria, Canada, 2020, pp. 1–5, <https://doi.org/10.1109/VTC2020-Fall49728.2020.9348697>.
- [13] B. Zheng and R. Zhang, "Intelligent Reflecting Surface-Enhanced OFDM: Channel Estimation and Reflection Optimization," *IEEE Wireless Communications Letters*, vol. 9, no. 4, pp. 518–522, Apr. 2020, <https://doi.org/10.1109/LWC.2019.2961357>.
- [14] S. Zhang and R. Zhang, "Capacity Characterization for Intelligent Reflecting Surface Aided MIMO Communication," *IEEE Journal on Selected Areas in Communications*, vol. 38, no. 8, pp. 1823–1838, Dec. 2020, <https://doi.org/10.1109/JSAC.2020.3000814>.
- [15] S. Abeywickrama, R. Zhang, Q. Wu, and C. Yuen, "Intelligent Reflecting Surface: Practical Phase Shift Model and Beamforming Optimization," *IEEE Transactions on Communications*, vol. 68, no. 9, pp. 5849–5863, Sep. 2020, <https://doi.org/10.1109/TCOMM.2020.3001125>.
- [16] C. Huang, G. Chen, Y. Gong, M. Wen, and J. A. Chambers, "Deep Reinforcement Learning-Based Relay Selection in Intelligent Reflecting Surface Assisted Cooperative Networks," *IEEE Wireless Communications Letters*, vol. 10, no. 5, pp. 1036–1040, Feb. 2021, <https://doi.org/10.1109/LWC.2021.3056620>.
- [17] K. Stylianopoulos, G. Alexandropoulos, C. Huang, C. Yuen, M. Bennis, and M. Debbah, "Deep Contextual Bandits for Orchestrating Multi-User MISO Systems with Multiple RISs," in *ICC 2022 - IEEE International Conference on Communications*, Seoul, Korea (South), May 2022, pp. 1556–1561, <https://doi.org/10.1109/ICC45855.2022.9838369>.
- [18] D. Pereira-Ruisánchez, Ó. Fresnedo, D. Pérez-Adán, and L. Castedo, "Deep Contextual Bandit and Reinforcement Learning for IRS-Assisted MU-MIMO Systems," *IEEE Transactions on Vehicular Technology*, vol. 72, no. 7, pp. 9099–9114, Jul. 2023, <https://doi.org/10.1109/TVT.2023.3249353>.
- [19] G. C. Alexandropoulos, K. Stylianopoulos, C. Huang, C. Yuen, M. Bennis, and M. Debbah, "Pervasive Machine Learning for Smart Radio Environments Enabled by Reconfigurable Intelligent Surfaces," *Proceedings of the IEEE*, vol. 110, no. 9, pp. 1494–1525, Sep. 2022, <https://doi.org/10.1109/JPROC.2022.3174030>.
- [20] Y. Jin, J. Zhang, B. Ai, and X. Zhang, "Channel Estimation for mmWave Massive MIMO With Convolutional Blind Denoising Network," *IEEE Communications Letters*, vol. 24, no. 1, pp. 95–98, Jan. 2020, <https://doi.org/10.1109/LCOMM.2019.2952845>.
- [21] Y. Jin *et al.*, "Multiple Residual Dense Networks for Reconfigurable Intelligent Surfaces Cascaded Channel Estimation," *IEEE Transactions on Vehicular Technology*, vol. 71, no. 2, pp. 2134–2139, Oct. 2022, <https://doi.org/10.1109/TVT.2021.3132305>.
- [22] S. Liu, Z. Gao, J. Zhang, M. D. Renzo, and M. S. Alouini, "Deep Denoising Neural Network Assisted Compressive Channel Estimation for mmWave Intelligent Reflecting Surfaces," *IEEE Transactions on Vehicular Technology*, vol. 69, no. 8, pp. 9223–9228, Dec. 2020, <https://doi.org/10.1109/TVT.2020.3005402>.
- [23] E. Vlachos, G. C. Alexandropoulos, and J. Thompson, "Massive MIMO Channel Estimation for Millimeter Wave Systems via Matrix Completion," *IEEE Signal Processing Letters*, vol. 25, no. 11, pp. 1675–1679, Aug. 2018, <https://doi.org/10.1109/LSP.2018.2870533>.
- [24] L. Wei, C. Huang, G. C. Alexandropoulos, C. Yuen, Z. Zhang, and M. Debbah, "Channel Estimation for RIS-Empowered Multi-User MISO Wireless Communications," *IEEE Transactions on Communications*, vol. 69, no. 6, pp. 4144–4157, Jun. 2021, <https://doi.org/10.1109/TCOMM.2021.3063236>.
- [25] H. B. Mahesh, G. F. A. Ahammed, and S. M. Usha, "Design and Performance Analysis of Massive MIMO Modeling with Reflected Intelligent Surface to Enhance the Capacity of 6G Networks," *Engineering, Technology & Applied Science Research*, vol. 13, no. 6, pp. 12068–12073, Dec. 2023, <https://doi.org/10.48084/etasr.6234>.